Nanoscale

PAPER

View Article Online
View Journal | View Issue

Cite this: *Nanoscale*, 2025, **17**, 27506

Cationic amino acid-engineered peptide hydrogels for sustained and potent antigen delivery enabling single-administration vaccination

Jingjing Zhou, Jiaxi Yu, Shengying Zhang, Zhidong Teng, Haoyue Zang, Mingyang Zhang, Shiqi Sun* and Huichen Guo *

Received 8th September 2025,
Accepted 5th November 2025

DOI: 10.1039/d5nr03790e

rsc.li/nanoscale

Peptide hydrogels have attracted considerable interest as vaccine delivery systems. This study systematically investigates how cationic residues affect peptide hydrogel-mediated antigen delivery and immune response, as well as the possibility of achieving single-dose immunization. Here, peptide Jelleine-1 (J-1) was employed as a template to generate peptide J-2, in which the type of cationic amino acid was modified, and peptide J-3, which lacks cationic residues. Peptides J-1, J-2, and J-3 self-assembled in antigen solutions to form hydrogel vaccines Gel 1, Gel 2, and Gel 3, respectively. Their mechanical properties, sustained antigen release, antigen uptake, and immune responses following single-dose administration were investigated. Results show that electrostatic interactions between cationic nanofibers and negatively charged antigens in Gel 1 and Gel 2 facilitated sustained antigen release and enrichment of macrophages and dendritic cells (DCs) at the injection site. Furthermore, cationic peptides induced DC membrane depolarization, which enhanced antigen uptake by 1.6-fold (Gel 1) and 1.8-fold (Gel 2) and increased DC activation by 3.3-fold and 3.1-fold, respectively. Ultimately, single administration of cationic peptide hydrogel vaccines Gel 1 and Gel 2 induced robust, long-lasting (up to 140 days), and balanced Th1/Th2 immune responses. These findings offer a conceptual framework for designing single-administration vaccine delivery systems.

1 Introduction

Vaccines play a critical role in public health and the prevention of infectious diseases. The primary goal of vaccination is to elicit a robust and long-lasting immune response against specific pathogens. During primary immunization, the immune system first encounters an antigen, learns to recognize it, and subsequently mounts an antigen-specific immune response.[1] However, most licensed vaccines require multiple booster doses, where repeated antigen exposure is necessary to achieve effective and durable immune protection. Broad vaccine deployment is limited by high vaccination costs, poor patient adherence to multi-dose regimens, and restricted access to healthcare in developing countries.[2] Therefore, the development of single-dose vaccines is an urgent challenge in current vaccine research. Sustained antigen release has been shown to enhance immune efficacy by extending antigen exposure.[3] For example, Crotty *et al.* recently reported that continuous delivery of an HIV Env immunogen over two weeks elicited germinal center responses lasting at least six months.[4] These findings suggest that controlled antigen-release systems can persistently activate immune responses, generating robust and sustained antigen-specific immune memory. Advances in materials science have led to the development of various biomaterials to enhance vaccine potency, such as nanoparticles, liposomes, and hydrogels.[5–7]

Hydrogels have received considerable attention in biomedical applications, including regenerative medicine, three-dimensional (3D) cell culture, and drug delivery, due to their excellent biocompatibility and structural versatility.[8,9] Theoretically, solid-like hydrogels may establish an inflammatory niche and serve as an antigen depot at the injection site, allowing gradual antigen release and persistent immune stimulation. Additionally, their fibrous microarchitecture recapitulates features of the extracellular matrix, providing a supportive scaffold for immune cell recruitment.[10] Moreover, the porous 3D network of hydrogels promotes immune cell migration, *in situ* antigen presentation, and the targeted transport of mature dendritic cells (DCs) to lymph nodes.[11,12] Taken together, hydrogels are thus considered among the most promising platforms for sustained antigen delivery.[13] Peptide-based nanomaterials represent promising antigen delivery platforms due to their biocompatibility, programmable sequences, and

State Key Laboratory for Animal Disease Control and Prevention, College of Veterinary Medicine, Lanzhou University, Lanzhou Veterinary Research Institute, Chinese Academy of Agricultural Sciences, Lanzhou 730046, China.
E-mail: sunshiqi@caas.cn, guohuichen@caas.cn

ability to encapsulate antigens through simple physical entrapment.[14–17] Collier *et al.* demonstrated that Q11 peptide nanofibers, without additional adjuvants, enhance antigen uptake, DC activation, and germinal center formation, thereby potentiating immune response.[18–20] Similarly, Yang *et al.* established that hydrogels formed by Npx-GFFY and its analogs could encapsulate diverse antigens, eliciting potent immune responses through simple physical encapsulation.[21–24] Despite these advantages, nearly all reported peptide hydrogel vaccines require multiple immunizations to achieve optimal immunogenicity, likely due to insufficient specific interactions between the antigen and the hydrogel network. Cationic amino acids play a key role in the physicochemical properties of peptides, yet their impact on antigen delivery mediated by peptide hydrogels remains unclear.[25]

Subunit antigens are increasingly favored for their cost-effectiveness and favorable safety profile. In particular, virus-like particles (VLPs) formed by self-assembly of viral capsid proteins, which are similar in size and morphology to natural pathogens, have unique immunological advantages.[26] In our previous study, we successfully generated foot-and-mouth disease (FMD) VLPs with an average diameter of 25 nm using an *E. coli* expression system, which elicited robust protective immune responses in guinea pigs, swine, and cattle.[27] Notably, most subunit antigens, including FMD VLPs, possess an intrinsic anionic surface charge. Electrostatic interactions between FMD VLPs and cationic peptides may therefore enable efficient antigen loading and suppress rapid antigen release. Besides, cationic motifs have been shown to facilitate cellular uptake and efficient delivery of various cargos, such as mRNA and proteins.[28] Furthermore, histidine residues within peptide sequences undergo protonation under acidic conditions, enhancing endosomal escape and cytosolic delivery. Although antigen depots primarily induce Th2-type humoral responses,[29] the cytosolic delivery of the antigenic properties of cationic peptides may also promote Th1-type cellular immune responses.

In this study, we systematically investigated the effect of cationic peptide hydrogels on sustained and efficient antigen delivery and the resulting immune response. Cationic peptide

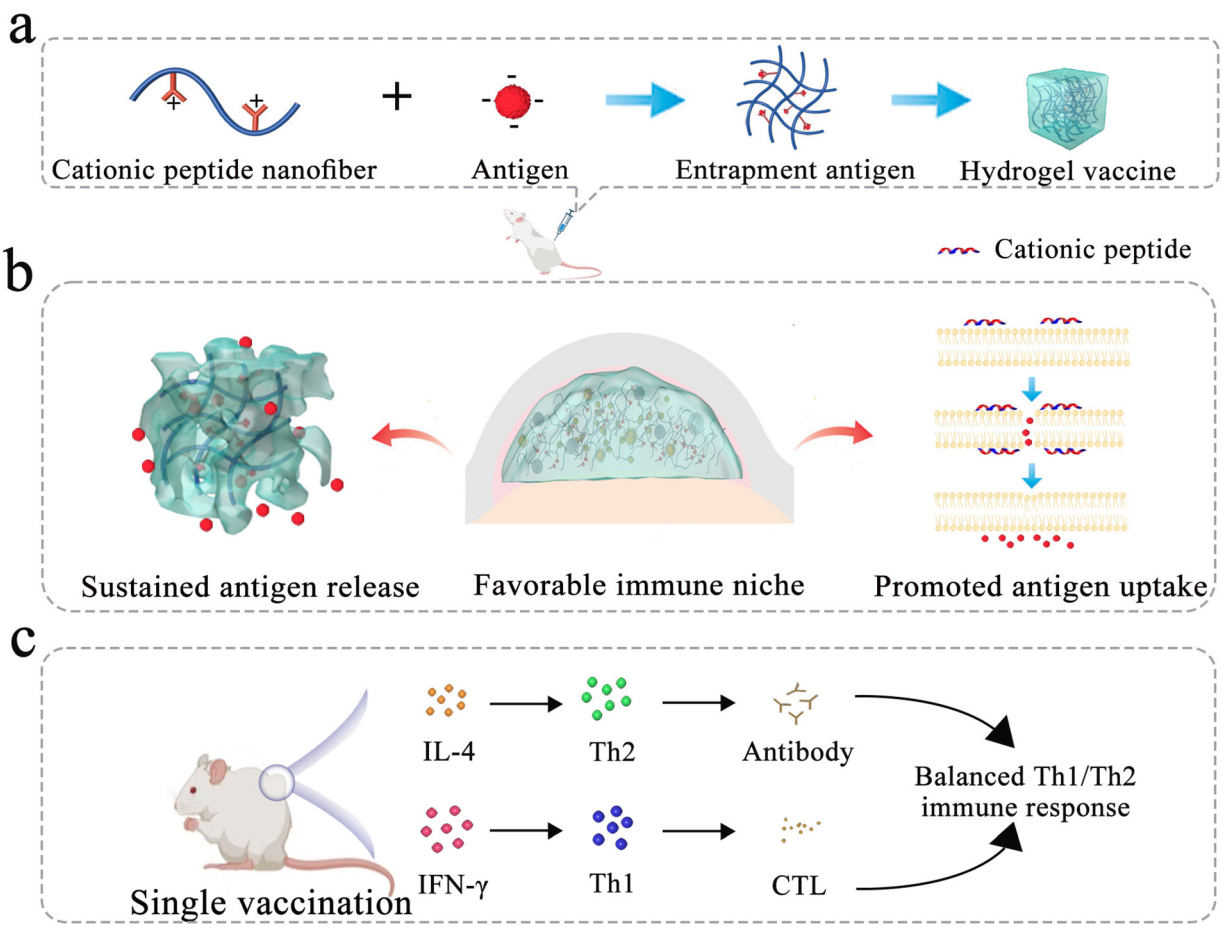

Scheme 1 Schematic illustration of cationic peptide hydrogel vaccine preparation and its induced immune responses. (a) Cationic peptides spontaneously self-assemble in the antigen solution, forming hydrogel vaccines. (b) Upon subcutaneous injection, the cationic peptide hydrogel forms a favorable immune niche at the injection site, enabling sustained antigen release and membrane depolarization-mediated antigen uptake. (c) Following a single administration, the cationic peptide hydrogel markedly enhances antigen-specific cellular and humoral immune responses, resulting in a more balanced Th1/Th2 profile.

Jelleine-1 (PFKLSLHL-NH_2, J-1), known for its ability to self-assemble into hydrogels in various salt solutions,[30–32] served as the template. Analogs J-2 (PFRLSLHL-NH_2) and J-3 (PFLSLHL-NH_2) were generated by modifying or removing the cationic residues in the J-1 sequence. Peptides J-1, J-2, and J-3 self-assembled within antigen solutions to form hydrogel vaccines Gel 1, Gel 2, and Gel 3, respectively, without the need for cross-linking agents. The mechanical properties and cytocompatibility of these hydrogels were characterized, followed by assessment of their sustained antigen release profiles both *in vitro* and *in vivo*. We further evaluated their effects on antigen uptake, DC maturation, and antigen presentation. Finally, the antigen-specific humoral and cellular immune responses induced in mice after a single immunization were analyzed. This work demonstrates how cationic amino acid residues in peptide hydrogels can promote sustained and efficient antigen delivery and shape the magnitude and quality of antigen-specific immune responses *in vivo* (Scheme 1).

2 Experimental

2.1 Materials

Calcein acetoxymethyl ester/propidium iodide (calcein-AM/PI) live/dead cell double staining kits, fluorescein isothiocyanate (FITC)-conjugated ovalbumin (OVA), cyanine 5 (Cy5)-conjugated OVA, and Hanks' digest solution were obtained from Beijing Solarbio Science & Technology Co., Ltd (China). Flow cytometry antibodies were purchased from Becton, Dickinson, and Company (USA). ELISA kits for the detection of O-type-specific antibodies against foot-and-mouth disease (FMD) virus were supplied by Lanzhou Veterinary Research Institute (China). ELISpot kits were provided by Mabtech (Sweden).

2.2 Animals

Female BALB/c mice (6–8 weeks old) were purchased from the Laboratory Animal Center, Lanzhou Veterinary Research Institute, Chinese Academy of Agricultural Sciences. All animals were housed under standard specific pathogen-free conditions with *ad libitum* access to food and water. Every effort was made to minimize the number of animals used and to reduce suffering. All procedures were conducted in compliance with the European Communities Council Directive 86/609/EEC and were approved by the Animal Administration and Ethics Committee of Lanzhou Veterinary Research Institute, Chinese Academy of Agricultural Sciences (Permit No. LVRIAEC-2024-027).

2.3 Peptide synthesis and hydrogel formation

All peptides (J-1, J-2, and J-3) were synthesized by Hefei Scierbio Co., Ltd. Structural identity of the peptides was confirmed by single quadrupole mass spectrometry (ZQ-2000, Waters, USA), and peptide purity was determined by reversed-phase high-performance liquid chromatography (HPLC) (SIL-16, Shimadzu, Japan). Lyophilized peptide powders were dissolved in DMSO to prepare 100 mM stock solutions. Each stock solution (100 μL) was then diluted with 900 μL of phosphate-buffered saline (PBS; pH 7.4), with or without antigen, to yield a final peptide concentration of 10 mM. After mixing and gentle shaking, transparent hydrogels formed within 5 min. Subsequently, the pH values of all resulting hydrogels were measured.

2.4 Fourier transform infrared (FTIR) analysis

The secondary structure of the peptides after gelation was investigated using an FTIR spectrometer (TENSOR 27, Bruker, Germany). The lyophilized powders of gel 1, gel 2, and gel 3 were separately mixed with potassium bromide (KBr) and pressed into pellets for measurement. FTIR spectra were then recorded over a wavenumber range of 1000–1800 cm^{-1}.

2.5 Rheological properties

The storage modulus (G') and loss modulus (G'') of the hydrogels were measured using a HAAKE RS6000 rheometer (Thermo, USA). A 35 mm parallel plate with a 1 mm gap was employed. The linear viscoelastic range (LVR) was determined using dynamic strain sweeps from 0.1% to 1000% at 1 Hz. Time sweeps were performed at 1% strain and 1 Hz for 15 min. Frequency sweeps were conducted from 1 to 100 rad per s at 1% strain. Injectability was assessed by step-strain assays, with G' and G'' measured at low strain (1%) for 5 min, followed by high strain (100%) for 1 min, repeated for three cycles. All rheological measurements were performed at 25 °C.

2.6 Extrusion test

Rhodamine B was incorporated into Gel 1 during preparation. The hydrogel was then loaded into a syringe fitted with a 0.45 mm diameter needle and extruded to write the word "Gel". The resulting pattern was photographed for documentation.

2.7 Cytotoxicity

Cytotoxicity of the hydrogels was evaluated using the MTS assay in Marc 145 cells. 1×10^4 cells per well were seeded in 96-well plates. After cell attachment, 100 μL of hydrogel extract was added to each well. Following 24, 48, and 72 h incubation at 37 °C, 10 μL of MTS reagent was added, and the cells were further incubated for 2 h. Absorbance at 490 nm was measured using a Synergy H1 microplate reader (BioTek, USA) to determine cell viability. Tissue culture plate (TCP) wells served as controls. For the live/dead assay, the cells were washed with PBS after incubation with the hydrogel extract and stained sequentially with calcein-AM (2 μM, 30 min) and PI (4.5 μM, 15 min) at 37 °C. Morphology and viability were observed under a fluorescence microscope.

2.8 Blood compatibility

Mouse red blood cells were used to assess hemocompatibility. Hydrogels were incubated with 400 μL of PBS for 24 h in 1.5 mL EP tubes. Then, 500 μL of 8% (v/v) mouse red blood cell suspension was added to the above hydrogels. PBS and 1% Triton X-100 served as negative and positive controls, respect-

ively. After incubation for 1 h at 37 °C and centrifugation at 1500*g* for 15 min, the supernatants were collected, and absorbance at 490 nm was measured to calculate hemolysis rates. The integrity of red blood cells was assessed microscopically.

2.9 Antigen release *in vitro*

The peptide stock solution (50 μL) was diluted with 450 μL of PBS containing FITC-OVA (5 μg mL^{-1}) to prepare hydrogels. Then, 400 μL of PBS (pH 7.4) was layered above the hydrogel and incubated at 37 °C for 24 h. The PBS supernatant was collected and the fluorescence intensity was measured to quantify released FITC-OVA. Fresh PBS was then added, and the process was repeated until the hydrogel was no longer visible.

2.10 Antigen release assay *in vivo*

In vivo sustained antigen release was monitored using a biological imaging system (AniView 100, BLT, China). The mice were subcutaneously injected with 200 μL of hydrogel containing Cy5-OVA. At 3, 72, 168, and 240 h post-injection, the mice were anesthetized with isoflurane, and the fluorescence at the injection site was imaged. The fluorescence intensity and luminescence area were analyzed using AniView software.

2.11 Cell recruitment *in vitro*

DC 2.4 cells were serum-starved in DMEM for 24 h before the assay. Hydrogels were placed in the lower chamber, and 600 μL of medium with 10% FBS was added to the above hydrogels. A transwell insert (8.0 μm pore size) was used to separate chambers. 1×10^5 DC 2.4 cells per insert were added to the upper chamber and incubated at 37 °C and 5% CO_2 for 24 h. The recruited cells in the lower chamber were counted by optical microscopy.

2.12 Cell recruitment and infiltration *in vivo*

The total number and phenotypes of cells recruited into the hydrogels were determined *in vivo*. Five days after subcutaneous injection of 200 μL of hydrogels, nodules were aseptically excised and mechanically dissociated and then placed in 10 mL of Hanks' digest solution to generate single-cell suspensions. The total cell count was determined, and the density of the suspension was adjusted to 1×10^6 cells per well for subsequent analysis. The proportions of $CD4^+$ T cells ($CD3^+CD4^+$), $CD8^+$ T cells ($CD3^+CD8^+$), B cells ($CD3^-B220^+$), dendritic cells ($CD11c^+$), and macrophages ($CD11b^+F4/80^+$) were analyzed by flow cytometry to characterize cell recruitment and infiltration.

2.13 Cell membrane depolarization

Membrane depolarization of DC 2.4 cells induced by hydrogels was assessed using a bis(1,3-dibutylbarbituric acid) trimethine oxonol ($DiBAC_4(3)$) fluorescent probe. DC 2.4 cells were incubated with 10 μM $DiBAC_4(3)$ for 30 min, followed by hydrogel exposure for 2 h. The fluorescence intensity was measured at 37 °C (excitation/emission: 490/516 nm). Quantitative analysis was performed to compare the fluorescence intensities of the hydrogel-treated groups and the untreated controls, indicating changes in membrane potential.

2.14 Antigen uptake

To examine cellular antigen uptake, hydrogels containing FITC-OVA were incubated with DC 2.4 cells for 12 h. After incubation, the cells were collected, washed, fixed with 4% paraformaldehyde, and stained with DAPI for nuclear visualization. Antigen uptake was then assessed and imaged by confocal laser scanning microscopy (CLSM; Leica DM6000, Germany).

2.15 DC maturation and antigen presentation

Activation and antigen presentation by DC 2.4 cells were evaluated by flow cytometry following 24 h incubation with hydrogels. The frequencies of $CD80^+CD86^+$, MHC-I^+, and MHC-II^+ cells within the $CD11c^+$ population were quantified to determine DC maturation and antigen-presenting capability.

2.16 Antigen-specific immune response

Female BALB/c mice (6–8 weeks old) received subcutaneous injections of 200 μL of PBS, 200 μL of PBS containing 10 μg of FMD VLPs, or 200 μL of Gel 1, Gel 2, or Gel 3 each containing 10 μg of FMD VLP. Blood samples were collected at days 7, 14, 28, 56, 112, and 140 post-immunization, and serum was isolated by centrifugation (4000 rpm, 20 min, 4 °C) and stored at −20 °C. ELISA was performed to detect specific antibody levels in mouse serum. Serum was incubated with inactivated FMDV-type O antigen at 4 °C for 12 h, and specific antibody detection followed the kit instructions. Serum IgG1 and IgG2a concentrations were quantified according to the manufacturer's protocols. Spleens were collected on day 56 post-immunization, and single-cell suspensions were prepared. The splenic lymphocyte density was adjusted to 3×10^5 cells per well for ELISpot assays detecting interleukin-4 (IL-4) and interferon-gamma (IFN-γ) secretion, according to the manufacturer's instructions, and reading with an AID ELISpot reader. For proliferation assays, the lymphocyte density was adjusted to 2×10^5 cells per well and cell proliferation was assessed using the MTS assay. The splenic lymphocyte density was adjusted to 1×10^6 cells per well, and flow cytometry was performed to determine the proportions of T follicular helper (Tfh, $CD3^+CD4^+PD\text{-}1^+CXCR5^+$) cells and cytotoxic T lymphocytes (CTL, $CD3^+CD8^+GZMB^+$).

2.17 Statistical analysis

Data were analyzed using GraphPad Prism 8.0 and are presented as the mean ± SEM. Unpaired, independent Student's *t*-tests (two-tailed) were used to compare differences between two groups. *P* values less than 0.05 were considered statistically significant.

3 Results and discussion

3.1 Synthesis of peptides and preparation of hydrogels

In this study, two analogs of peptide J-1 were designed to investigate the functional role of the cationic residue. As illustrated in Fig. 1a, J-2 was generated by substituting lysine (Lys) with arginine (Arg), while J-3 was created by deleting this

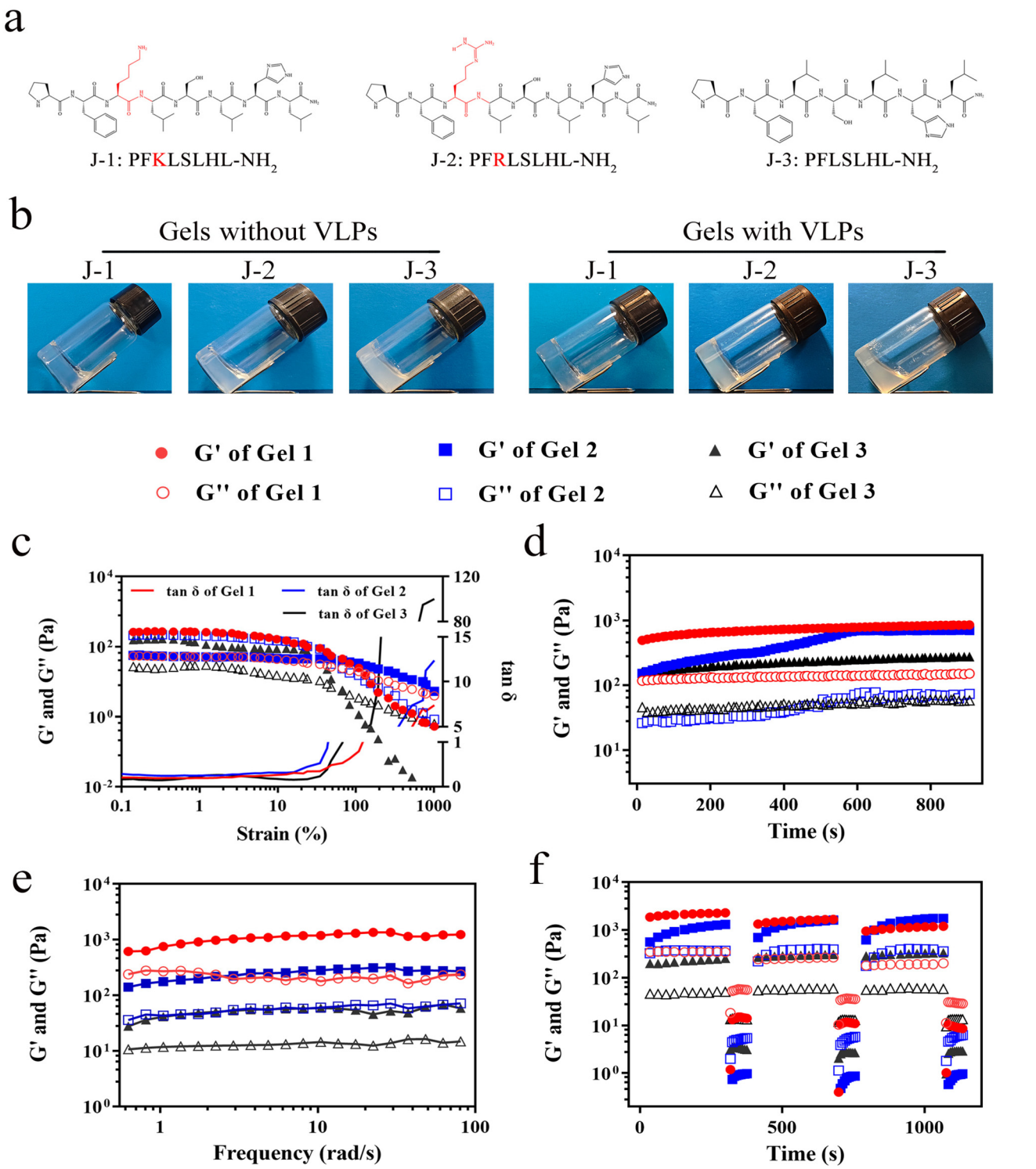

Fig. 1 Preparation and rheological characterization of Gel 1, Gel 2, and Gel 3. (a) Chemical structures of peptides J-1, J-2, and J-3. (b) Hydrogel formation of peptides J-1, J-2, and J-3 in PBS (left) and PBS containing antigen (right). (c) Strain sweep from 0.1% to 1000% at 1 Hz. (d) Time sweep at 1% strain and 1 Hz for 15 min. (e) Frequency sweep from 0.1 to 100 rad per s at 1% strain. (f) Step-strain test: alternating 1% strain (300 s) and 100% strain (60 s), repeated for three cycles.

Table 1 The sequences and physicochemical properties of peptides

Peptide	Sequence	Theoretical MW	Measured MW[a]	Retention time[b]	Purity[b]
J-1	PFKLSLHL-NH_2	952.59	953.81	16.149	95.884%
J-2	PFRLSLHL-NH_2	980.35	981.35	16.432	98.515%
J-3	PFLSLHL-NH_2	824.60	825.45	12.984	95.49%

[a] Measured molecular weights (MWs) of peptides J-1, J-2 and J-3 were defined by MS. [b] Retention time and purity of peptides J-1, J-2, and J-3 were determined by RP-HPLC.

residue. All these peptides were synthesized *via* classical solid-phase peptide synthesis. Structural identity was verified by MS (Table 1 and Fig. S1–S3), and purity was assessed by HPLC. All final compounds demonstrated a purity exceeding 95% (Table 1 and Fig. S4–S6). Then, each peptide was dispersed in 10 mM PBS (pH 7.4), gently vortexed, and left to stand to assess hydrogel formation. Fig. 1b shows that under these conditions, J-1, J-2, and J-3 each formed stable hydrogels, designated as gel 1 (pH 7.6), gel 2 (pH 7.4), and gel 3 (pH 7.8), respectively. We next utilized FTIR spectroscopy to investigate the secondary structure of the peptides in the hydrogel state. As shown in Fig. S7, FTIR spectra revealed a characteristic negative peak at 1620–1630 cm^{-1} for all peptides, confirming a β-sheet conformation. Additionally, a weak shoulder near 1690 cm^{-1} indicated an antiparallel arrangement of the β-sheets.[33] Notably, the addition of FMD VLP antigen (50 μg mL^{-1}) did not interfere with hydrogel formation, with J-1, J-2, and J-3 all forming stable hydrogels, designated as Gel 1 (pH 7.5), Gel 2 (pH 7.8), and Gel 3 (pH 7.8), respectively, in PBS containing the antigen (Fig. 1b). Therefore, Gel 1, Gel 2, and Gel 3 were generated by physically mixing peptide and antigen solutions, without the use of any cross-linkers. Compared with some hydrogels that often require complex conditions (such as organic/aqueous phase interfaces, thermal cycling, freeze-drying, protease, or surfactant treatments),[34] the approach used here is notably simple. Cationic amino acids confer a positive surface charge to the peptide nanofibers, promoting electrostatic interactions essential for hydrogel formation in some peptide-based systems.[35–37] However, our previous work established that hydrophobic interactions and intermolecular hydrogen bonding are the principal drivers of the self-assembly of the J-1 hydrogel primarily, which are contributed by phenylalanine, leucine, and histidine.[31] Therefore, substitution or removal of cationic amino acids did not substantially impair hydrogel formation, as confirmed by the ability of both J-2 and J-3 to form hydrogels under the same conditions.

3.2 Cationic Gel 1 and Gel 2 exhibit excellent mechanical properties

The mechanical strength of hydrogel vaccines is critical for establishing a stable antigen depot and enabling sustained antigen release following subcutaneous implantation.[38] Adequate mechanical strength also helps in minimizing adverse effects on surrounding tissues after injection.[39] In this study, we systematically evaluated the mechanical properties of all three hydrogels using a rheometer, focusing on G' and G'' as functions of strain, frequency, and time. The shear-thinning and self-healing properties of the hydrogels were further assessed by step-strain assays. As shown in Fig. 1c, the LVR for each hydrogel was defined by monitoring G' and G'' with increasing strain. All hydrogels maintained nearly constant G' and G'' with a $\tan\delta$ (G''/G') value of less than 1 over a strain range from 0.1% to 10%, indicating network stability within this range.[40] Consistent with the behavior of other peptide-based hydrogels, a marked decrease in both moduli was observed upon further increasing the strain.[41] Concurrently, the $\tan\delta$ value progressively increased and exceeded 1, confirming the onset of shear-thinning behavior. Fig. 1d demonstrates that, during a 15 min time sweep at 1% strain, all hydrogels exhibited plateau values for G' and G'', reflecting the formation of stable, well-connected peptide nanofiber networks. Importantly, for Gel 1 and Gel 2, G' was not only consistently higher than G'' but also reached values close to 1000 Pa, which is higher than the G' values reported for most peptide-based hydrogels.[42] This highlights their pronounced solid-like characteristics, supporting prolonged retention at the injection site. It should be noted that, as shown in Fig. S8, compared to the unloaded hydrogels (gel 1, gel 2, and gel 3), the antigen-loaded hydrogels (Gel 1, Gel 2, and Gel 3) exhibited a certain degree of reduction in G'. This indicates that the incorporation of antigens can compromise the mechanical strength of the hydrogels, likely because the partial positive charges on the cationic peptide nanofibers were neutralized by the negatively charged antigens, thereby weakening the interactions between the nanofibers. Frequency sweep analysis (Fig. 1e) revealed that G' remained significantly greater than G'' and both moduli were largely independent of frequency over the range of 0.1–100 rad per s, further highlighting the structural stability of all hydrogels. In the step-strain experiment (Fig. 1f), application of 100% strain led to G'' exceeding G', indicating network disruption. However, when strain was reduced back to 1%, all hydrogels rapidly regained their original mechanical properties, with G' exceeding G'' again. This rapid recovery after repeated cycles demonstrated robust self-healing ability, attributed to reversible noncovalent interactions among the peptide nanofibers. Furthermore, Gel 1 was extruded through a syringe needle with a diameter of 0.45 mm, producing a continuous filament without fracture (Fig. S9), which further confirmed the injectability of this hydrogel. Collectively, these results establish that the peptide hydrogels prepared in this study possess both shear-thinning and self-healing properties, which enable minimally invasive

administration by syringe injection. These hydrogels, due to their superior solid-like properties, do not diffuse rapidly after injection but instead form a robust depot at the site. This allows for sustained antigen release, creating a local microenvironment that favors immune cell recruitment and infiltration, thereby supporting *in situ* antigen processing and presentation.[43] Notably, Gel 3, which lacks cationic amino acids, exhibited the lowest mechanical strength in all rheological measurements, as evidenced by its consistently lowest G' values.

3.3 Biocompatibility of hydrogels *in vitro*

Prior to *in vivo* implantation, it is essential to evaluate the biocompatibility of hydrogels *in vitro.*[44] In this study, we assessed the safety of Gel 1, Gel 2, and Gel 3 using Marc 145 cells and mouse red blood cells. First, the hydrogels were co-incubated with Marc 145 cells, and cytotoxicity was evaluated by measuring cell viability. As shown in Fig. S10, none of the hydrogels exhibited adverse effects on Marc 145 cell growth, with cell viability exceeding 95% even after 72 h of co-incubation. To further confirm these results, live/dead cell staining was performed after hydrogel treatment. As illustrated in Fig. S11, both the morphology and density of Marc 145 cells exposed to the hydrogels were comparable to those of the control group. In addition, the cytotoxicity of all hydrogels was lower than that of their respective peptide monomers (Fig. S12), suggesting that supramolecular hydrogel formation reduces direct exposure of cells to free peptides and thus minimizes cytotoxicity. The blood compatibility of the hydrogels was further examined by co-incubating them with mouse red blood cells. Consistent with their excellent cytocompatibility, all tested hydrogels demonstrated outstanding hemocompatibility, as indicated by hemolysis rates below 5% (Fig. S13) and the preservation of intact erythrocyte morphology following hydrogel exposure (Fig. S14). Collectively, these results confirm that Gel 1, Gel 2, and Gel 3 possess favorable cytocompatibility and hemocompatibility, supporting their suitability for further *in vivo* application.

3.4 Cationic Gel 1 and Gel 2 facilitate the sustained antigen release *in vitro* and *in vivo*

Sustained antigen release simulates the course of natural viral infection by prolonging antigen presentation through continuous capture by APCs, thereby enabling persistent immune stimulation.[45] In this study, we evaluated the *in vitro* antigen release profiles of the hydrogels by monitoring the cumulative release of FITC-OVA as a model antigen. As shown in Fig. 2a, all hydrogels exhibited similar release patterns without burst release. Specifically, Gel 3 achieved complete FITC-OVA release within 12 days, whereas cationic Gel 1 and Gel 2 required 18 and 17 days, respectively, to reach full antigen release. These results indicate that the internal nanofiber network of the hydrogels effectively restricts rapid antigen diffusion, ensuring sustained antigen release. Notably, cationic Gel 1 and Gel 2 showed slower antigen release, which can be attributed to electrostatic interactions between the negatively charged antigen and the positively charged peptide nanofibers.

For hydrogel vaccines, antigen release *in vivo* is mainly governed by hydrogel erosion mediated by body fluids.[46] To compare the *in vivo* antigen release characteristics of the three hydrogels, we subcutaneously injected the mice with either Cy5-OVA in PBS or Cy5-OVA-loaded hydrogels and tracked the fluorescence signal at the injection site by *in vivo* bioimaging. As shown in Fig. 2b, the Cy5 fluorescence signal from the PBS group diminished rapidly, disappearing within 72 h (3 days) after injection. In contrast, all hydrogel groups exhibited a much slower decrease in fluorescence intensity, with a detectable signal remaining at the injection site even after 168 h (7 days). Importantly, the fluorescence signal decayed more slowly in cationic Gel 1 and Gel 2 compared to Gel 3 (Fig. 2c and d). This observation is consistent with our *in vitro* findings and suggests that the combination of electrostatic interactions between cationic nanofibers and negatively charged antigens, together with physical confinement by the nanofiber network, synergistically suppresses rapid antigen diffusion in Gel 1 and Gel 2. In contrast, Gel 3 relies solely on physical entrapment for antigen retention. These results demonstrate that cationic peptide hydrogels enable prolonged antigen retention at the injection site, providing sustained antigenic signals for immune cell recruitment.[47,48]

3.5 Cationic Gel 1 and Gel 2 promote the recruitment and infiltration of immune cells *in vivo*

The nanofiber network within the hydrogels structurally mimics the extracellular matrix, creating a biomimetic substrate that supports cell recruitment and migration.[49] To evaluate these properties, we first performed *in vitro* transwell assays to assess the cell-recruiting potential of the hydrogels. As shown in Fig. 3a, all three hydrogels significantly promoted DC migration relative to the control, demonstrating their capacity to enhance cell recruitment. However, no statistically significant differences in DC migration were observed among the hydrogel groups *in vitro*. The porous and uniform structure of peptide hydrogels also facilitates cellular infiltration into the matrix.[50] Subcutaneous implantation of hydrogels can thus establish a local immune microenvironment favorable for immune cell recruitment and antigen processing.[51] To assess this *in vivo*, we injected each hydrogel subcutaneously into the mice and harvested the resulting nodules to quantify infiltrated cells. As shown in Fig. 3b, all hydrogels formed visible nodules with pronounced cellular infiltration. Quantitative analysis (Fig. 3c) revealed that each hydrogel nodule contained over 5 million cells. Notably, cationic Gel 1 and Gel 2 supported 3.3-fold and 2.2-fold greater cell infiltration, respectively, than non-cationic Gel 3. This directly demonstrates that peptide hydrogels, particularly cationic variants, serve as efficient 3D scaffolds for host cell recruitment *in vivo*. To characterize the recruited cell populations, we performed flow cytometry on the cells infiltrating the hydrogels. As shown in Fig. 3d–f, 87.7% of cells infiltrating Gel 1 were immune cells, including DCs (64.9%), macrophages (20.5%), T cells (0.7%),

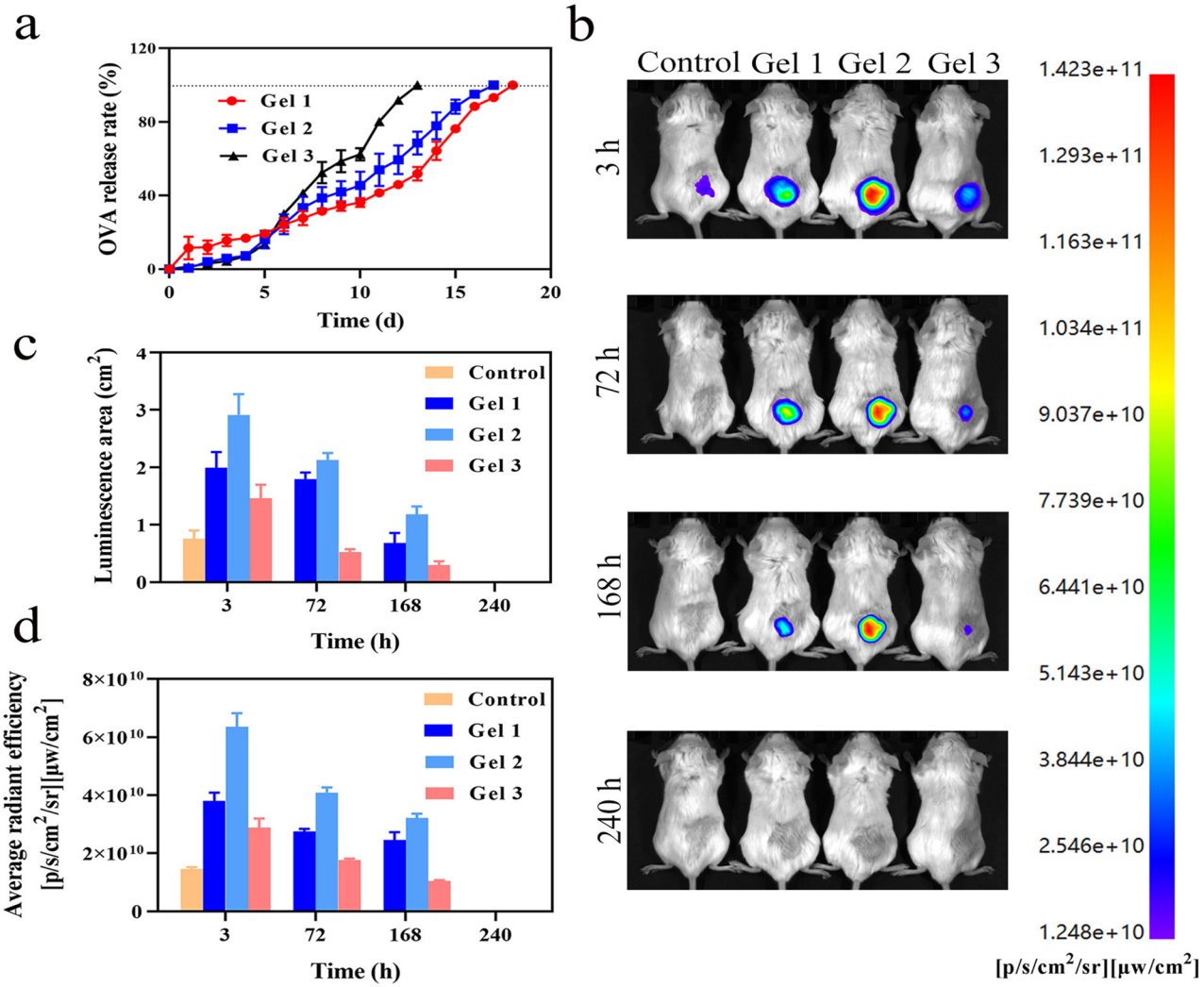

Fig. 2 Antigen release profiles of Gel 1, Gel 2, and Gel 3 *in vitro* and *in vivo*. (a) Cumulative release of the model antigen FITC-OVA from Gel 1, Gel 2, and Gel 3 *in vitro*. (b) *In vivo* fluorescence imaging of mice at various time points after subcutaneous administration of Cy5-OVA-loaded Gel 1, Gel 2, or Gel 3. (c and d) Quantitative analysis of the luminescence area (c) and fluorescence intensity (d) in each group. PBS solution containing FITC-OVA at an equivalent dose served as the control.

and B cells (1.6%). DCs and macrophages together accounted for 85.4% of the infiltrating population. Further analysis (Fig. S15) demonstrated that Gel 2 and Gel 3 also promoted recruitment and infiltration of DCs and macrophages.

3.6 Cationic Gel 1 and Gel 2 promote antigen uptake by depolarizing the cell membrane

Cationic amino acids are critical for the biological activity of peptides, as they modulate cell membrane dynamics through electrostatic interactions and significantly influence processes such as ion transport and endocytosis.[52] However, the effects of cationic peptide hydrogels on immune cell membranes and subsequent antigen internalization remain insufficiently characterized. In this study, we examined how the three peptide hydrogels influence the properties of the DC membrane and antigen uptake. As shown in Fig. 4a, cationic Gel 1 and Gel 2 induced significant changes in $DiBAC_4(3)$ fluorescence intensity, indicating pronounced membrane depolarization in DCs. Correspondingly, CLSM results (Fig. 4b and c) demonstrated that Gel 1 and Gel 2 enhanced OVA-FITC internalization by 1.6-fold and 1.8-fold, respectively, compared with non-cationic Gel 3. This enhancement in antigen internalization is attributed to cationic peptide-induced membrane depolarization *via* electrostatic interactions. Membrane depolarization likely increases transient membrane permeability and alters surface charge distribution, thereby facilitating the adsorption and internalization of negatively charged antigens.

3.7 Cationic Gel 1 and Gel 2 promote DC maturation

DC maturation is essential for initiating adaptive immune responses.[53,54] Given that cationic Gel 1 and Gel 2 enhance antigen uptake, we next assessed the effects of the three hydrogels on DC maturation and antigen presentation using flow

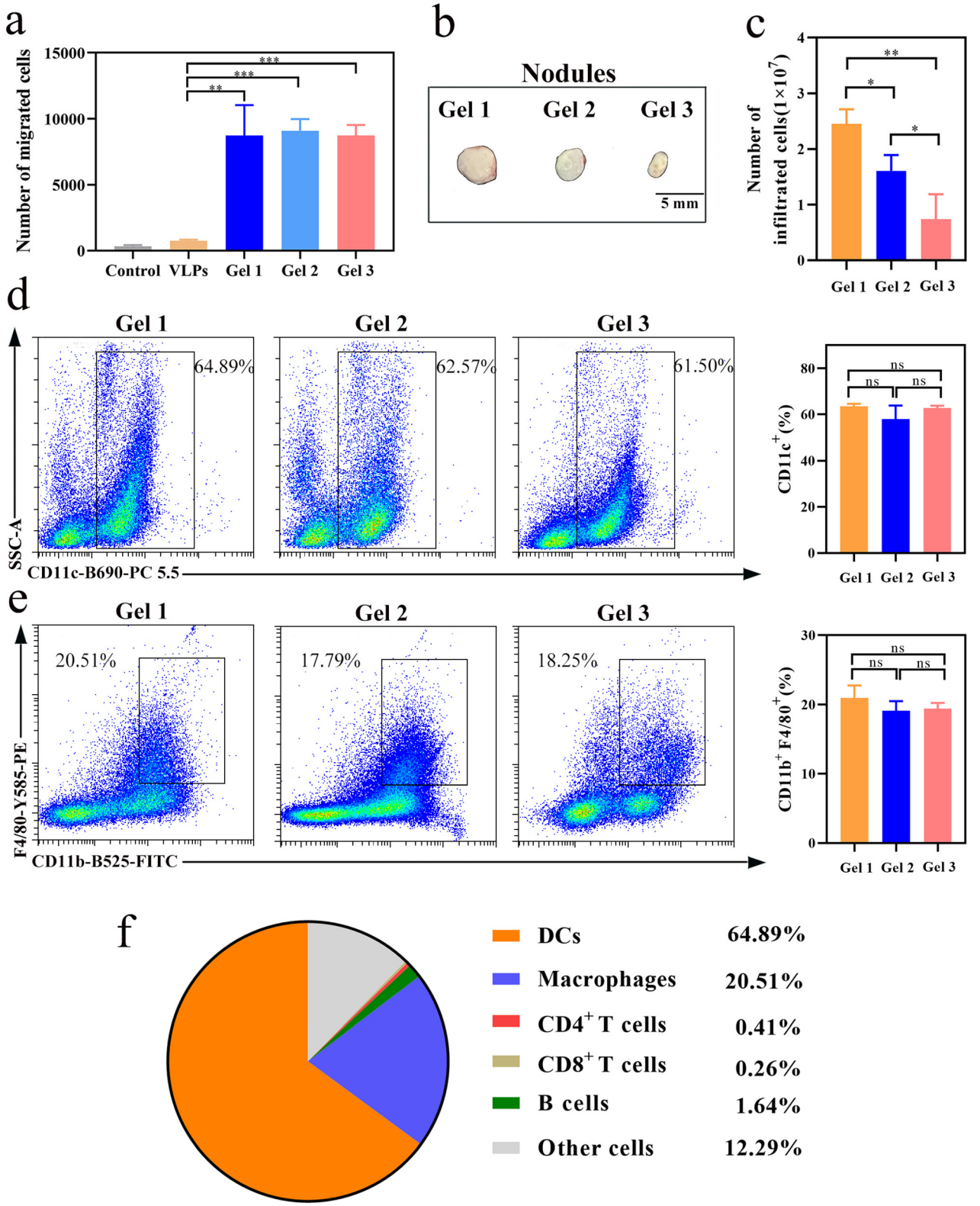

Fig. 3 Effects of cationic peptide hydrogels on immune cell recruitment *in vitro* and *in vivo*. (a) Number of DCs migrating toward the antigen, Gel 1, Gel 2, or Gel 3 *in vitro*. (b) Representative images of subcutaneous nodules formed 5 days after injection of Gel 1, Gel 2, or Gel 3. (c) Total cell number infiltrated into Gel 1, Gel 2, or Gel 3 *in vivo*. (d) Representative flow cytometry plots and proportion of $CD11c^+$ cells among the cells recruited by Gel 1. (e) Representative flow cytometry plots and proportion of $F4/80^+$ $CD11b^+$ cells among the cells recruited by Gel 1. (f) Frequency of DCs, macrophages, $CD4^+$ T cells, $CD8^+$ T cells, B cells, and other cells within the cell population recruited by Gel 1.

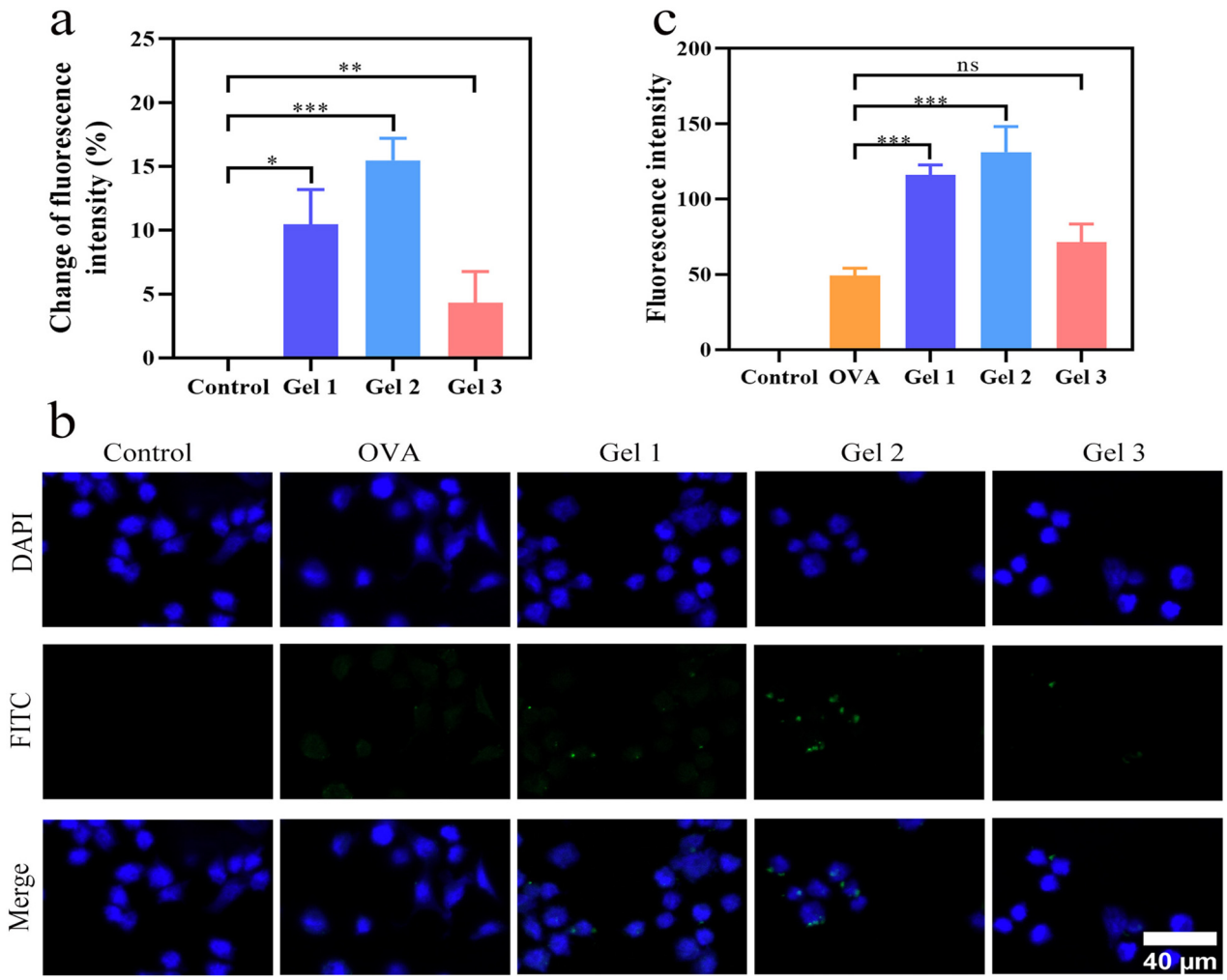

Fig. 4 Effects of peptide hydrogels on DC membrane depolarization and antigen uptake. (a) Degree of membrane depolarization in DCs following exposure to different hydrogels. (b) Representative CLSM images of DCs treated with Gel 1, Gel 2, or Gel 3 (DAPI: blue and FITC: green). Scale bar: 40 μm. (c) FITC-OVA fluorescence intensity of DCs from different treatment groups. DCs without FITC-OVA incubation served as the control.

cytometry. Quantitative analysis of surface co-stimulatory molecules revealed that DCs incubated with cationic Gel 1 and Gel 2 exhibited significantly upregulated CD80 and CD86 expressions compared with DCs treated with non-cationic Gel 3 (Fig. 5a), likely due to increased antigen uptake. Additionally, all three peptide hydrogels promoted increased expression of MHC-I (Fig. 5b) and MHC-II (Fig. 5c) in DCs. These findings indicate that cationic peptide hydrogels enhance DCs' maturation, while all hydrogels in this study facilitate the antigen presentation of both MHC-I and MHC-II, although the underlying mechanisms require further investigation.

3.8 Cationic Gel 1 and Gel 2 induce a potent humoral and cellular immune response following a single dose

In this study, peptide hydrogels, particularly cationic Gel 1 and Gel 2, showed clear advantages in sustained antigen release, immune cell recruitment, efficient antigen delivery, and DC activation. These characteristics prompted further evaluation of their effect on antigen-specific immune responses *in vivo*. To assess the potential of these hydrogels as single-dose vaccine delivery systems, the mice were immunized subcutaneously with a single injection of FMD VLPs formulated in either PBS or hydrogels. Serum samples were collected at predetermined time points (Fig. 6a), and anti-FMD VLP IgG levels were determined by ELISA. As shown in Fig. 6b, PBS-formulated antigen elicited only a transient humoral response. Although Gel 3 induced a significant increase in antigen-specific IgG levels compared to PBS at day 14, it failed to maintain high antibody titers over time, consistent with its suboptimal sustained release profile. In contrast, both cationic Gel 1 and Gel 2 induced sustained, high-titer antigen-specific IgG responses, with elevated antibody levels maintained throughout the 140-day post-immunization period. These results

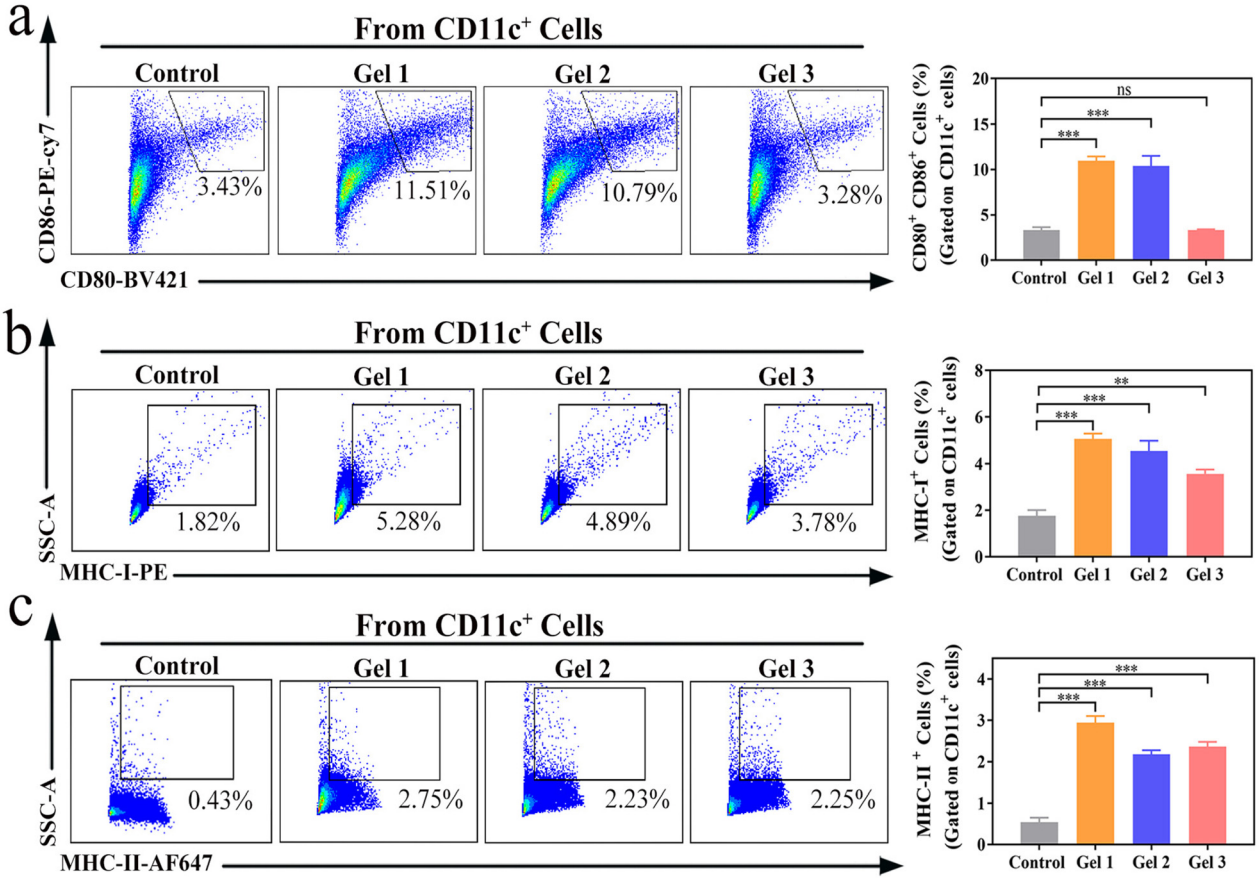

Fig. 5 Effect of cationic peptide hydrogels on DC activation and antigen presentation. (a) Representative plots and percentages of $CD80^+$ $CD86^+$ cells among the DCs treated with Gel 1, Gel 2, or Gel 3. (b) MHC-I expression in DCs after hydrogel treatment. (c) MHC-II expression in DCs after hydrogel treatment. DCs treated with culture medium served as the control group.

demonstrate that the cationic peptide hydrogels can maintain robust antibody titers for at least 140 days, effectively eliminating the need for booster injections.

Given the strong association between antigen-specific antibody production and Tfh cell differentiation,[55] splenic lymphocytes were isolated from immunized mice on day 56, and Tfh cell frequencies were quantified by flow cytometry. As shown in Fig. 6c, compared with PBS-formulated VLPs, cationic Gel 1 and Gel 2 increased Tfh cell numbers by 14.3-fold and 16.4-fold, respectively, whereas Gel 3 had little effect on Tfh cell levels. As biomarkers of Th2- and Th1-mediated immune responses, the IgG1 and IgG2a isotypes are essential for characterizing antigen-induced immune polarization.[56] To assess the immunomodulatory properties of these peptide hydrogels, we quantified both antibody subclasses and their related cytokine secretion profiles. As shown in Fig. 7a, PBS-formulated VLPs induced the lowest IgG1 production, whereas cationic Gel 1 and Gel 2 significantly elevated IgG1 levels. Fig. 7b demonstrates that this enhancement extended to IgG2a, indicating that cationic Gel 1 and Gel 2 concurrently enhanced both Th2- and Th1-mediated humoral responses. Notably, Gel 3 showed no significant modulatory effect on either IgG1 or IgG2a, consistent with its previously observed lower antigen retention and specific antibody levels. Analysis of the IgG2a/IgG1 ratio (Fig. 7c) revealed that PBS-formulated VLPs induced a distinctly Th2-skewed response (ratio < 1), whereas cationic Gel 1 and Gel 2 promoted both Th1 and Th2 responses, yielding a more balanced immune profile. These findings indicate that cationic peptide hydrogels have the unique ability to overcome the limitation of conventional antigen depots, which typically only amplify Th2-biased immunity.[57] Based on previous reports,[28] we propose that histidine residues in the peptide sequence become protonated within the acidic endosomal environment, leading to endosomal membrane disruption *via* the proton sponge effect and enabling cytosolic antigen delivery. To further characterize the immune polarization, we measured IL-4 and IFN-γ secretion by ELISpot, as these cytokines are critical mediators of Th2 and Th1 responses, respectively.[58] As shown in Fig. 7d, Gel 1 and Gel 2 significantly enhanced IL-4 production, increasing by 2.8-fold and 4.4-fold, respectively, compared to PBS-formulated VLPs, in line with the promotion of Th2 immunity. Fig. 7e shows that Gel 1 and Gel 2 amplified IFN-γ secretion by 2.2-fold and 2.4-fold, respect-

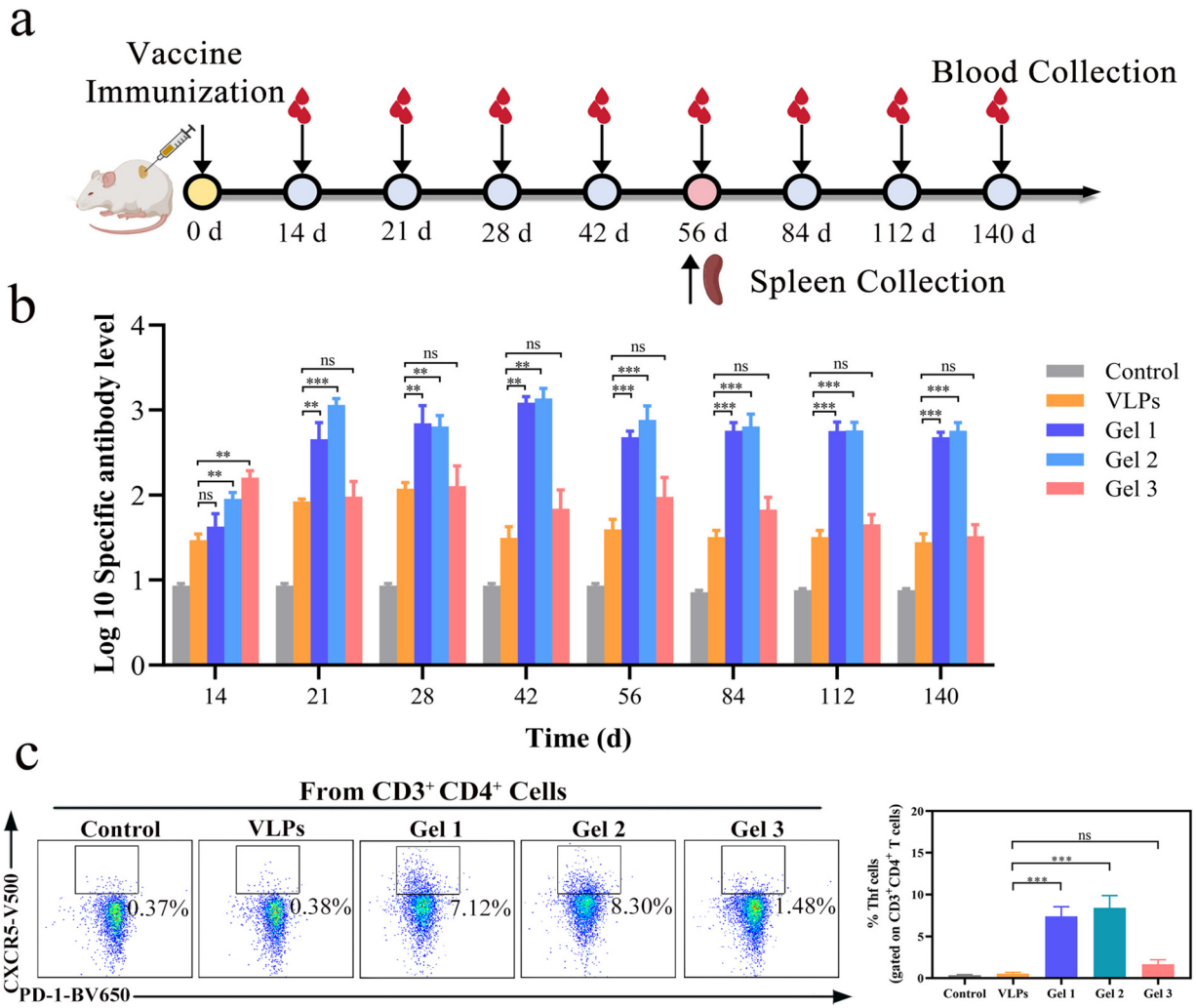

Fig. 6 Effect of cationic peptide hydrogels on antigen-specific humoral immune responses. (a) Schematic of the immunization schedule and sample collection time points for the blood and spleen. (b) Serum antigen-specific IgG levels in different immunization groups, determined by ELISA. (c) Representative plots and percentages of Tfh cells in the spleens of immunized mice on day 56. PBS-injected mice served as the control group.

ively, *versus* PBS-formulated VLPs, further confirming their capacity to enhance Th1 responses. In contrast, Gel 3 induced only minimal cytokine production.

The above findings demonstrate that cationic Gel 1 and Gel 2 significantly enhance Th1-biased immune responses, highlighting their potential for boosting cellular immunity. To further elucidate this effect, we quantified CTL populations in the spleens of immunized mice. As shown in Fig. 7f and g, Gel 1 and Gel 2 increased CTL proportions by 255% and 385%, respectively, compared to PBS-formulated VLPs, providing direct evidence for enhanced cellular immune activation. Although the mechanistic details remain to be fully defined, these results confirm the strong Th1-polarizing capacity of cationic peptide hydrogels. In contrast, most hydrogel-based vaccines primarily induce Th2-skewed humoral responses *via* the antigen depot effect.[13,57] Our results thus offer a unique approach for designing hydrogel vaccines capable of effectively promoting Th1 immunity.

Antigen-specific lymphocyte proliferation is a key indicator of immunological memory.[59] To assess the memory response induced by peptide hydrogel vaccination, splenocytes from immunized mice were re-stimulated with antigen *in vitro*. As shown in Fig. 7h, cationic Gel 1 and Gel 2 increased the proliferation index of splenocytes by 1.9-fold and 2.1-fold, respectively, relative to PBS-formulated VLPs, indicating a strong antigen-specific recall response. In contrast, Gel 3 did not significantly enhance splenocyte proliferation, reflecting its limited ability to induce immunological memory. This proliferative advantage highlights the capacity of cationic peptide hydrogels to establish durable immune memory, a foundational attribute for the *in vivo* efficacy of single-dose vaccines.

In summary, these results demonstrate that a single injection of cationic peptide hydrogel vaccines induces robust antigen-specific humoral and cellular immunity, emphasizing their substantial potential as delivery platforms for single-dose immunization.

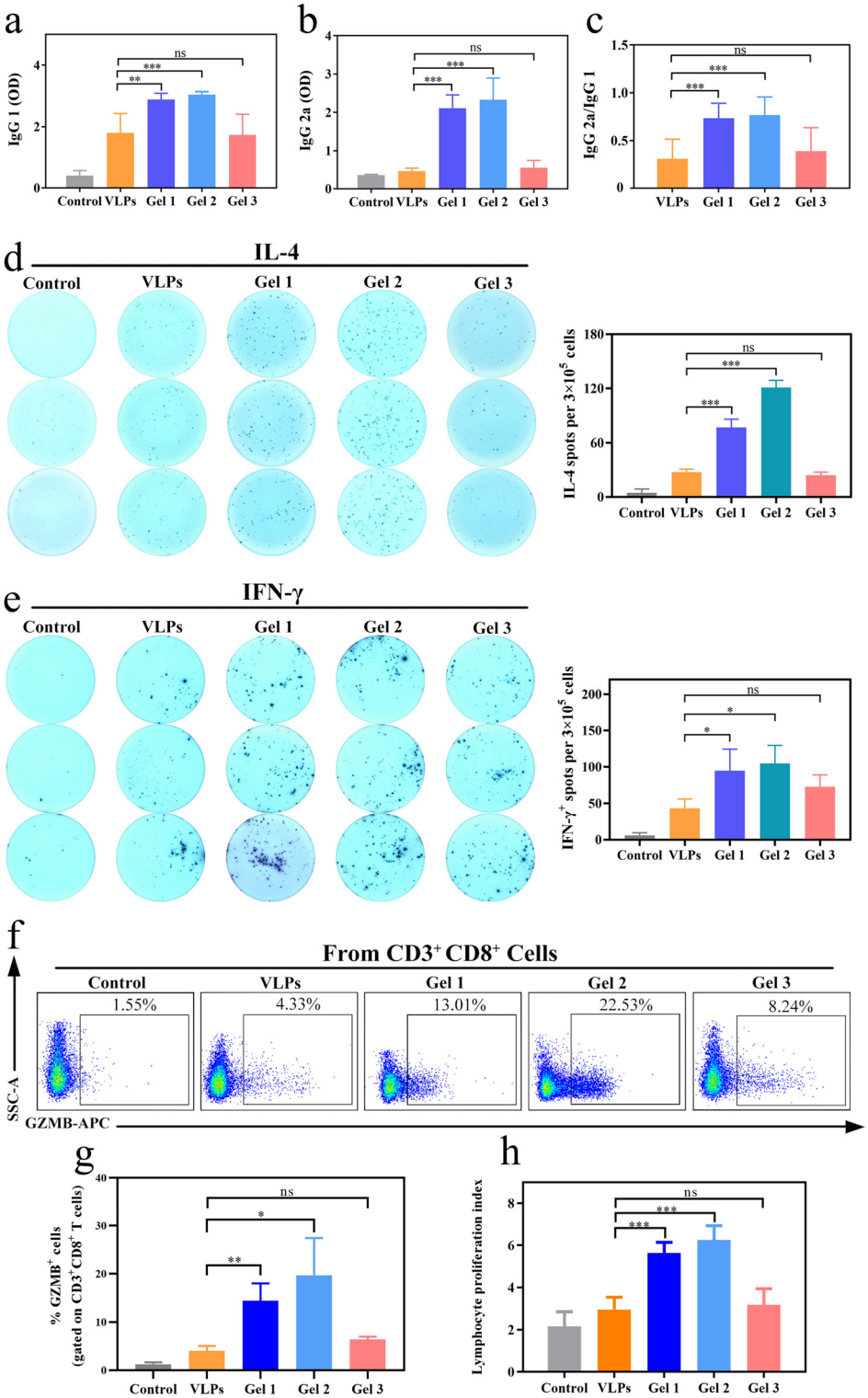

Fig. 7 Effect of cationic peptide hydrogels on Th1/Th2 immune responses. (a) IgG1 and (b) IgG2a levels in serum on day 56. (c) IgG2a/IgG1 ratio in different groups. Representative ELISpot images and quantification of splenocytes secreting (d) IL-4 and (e) IFN-γ. Representative flow cytometry plots (f) and quantification (g) of CTL in splenocytes. (h) Proliferation index of splenic lymphocytes in immunized mice. PBS-injected mice served as the control group.

4 Conclusions

In this study, we systematically examined the effects of cationic residues on antigen delivery and immune responses in peptide hydrogel vaccines. Using the naturally self-assembling peptide J-1 as a template, we generated analogues J-2 (with modified cationic residues) and J-3 (lacking cationic amino acids). All three peptides self-assembled in antigen solutions to directly form hydrogel vaccines (Gels 1–3). Compared to non-cationic Gel 3, both cationic Gel 1 and Gel 2 achieved sustained antigen release through a combination of electrostatic interactions between cationic nanofibers and antigens and physical confinement within the nanofiber network. This led to prolonged antigen availability, continuous immune cell recruitment, and the formation of a distinctive immune microenvironment enriched with APCs. Moreover, Gel 1 and Gel 2 induced DC membrane depolarization, thereby enhancing antigen internalization and enabling efficient antigen delivery. Therefore, a single immunization with cationic Gel 1 or Gel 2 generated stronger and more durable antibody titers, as well as a more balanced Th1/Th2 immune response. Collectively, these results demonstrate that cationic peptide hydrogels possess unique advantages in sustained antigen release and efficient antigen uptake, supporting their considerable potential as delivery platforms for single-dose vaccines.

Author contributions

Jingjing Zhou: investigation, methodology, formal analysis, validation, writing – original draft, and funding acquisition. Jiaxi Yu: methodology, formal analysis, and validation. Shengying Zhang: methodology and formal analysis. Zhidong Teng: methodology and validation. Haoyue Zang: methodology and formal analysis. Mingyang Zhang: methodology. Shiqi Sun and Huichen Guo: conceptualization, investigation, funding acquisition, and writing – review & editing.

Conflicts of interest

There are no conflicts to declare.

Data availability

All data supporting the findings of this study are available within the article and its supplementary information (SI). Supplementary information is available. See DOI: https://doi.org/10.1039/d5nr03790e.

Acknowledgements

This work was supported by grants from the National Natural Science Foundation of China (No. 32301127 and 32473012), the Natural Science Foundation of Gansu Province (No. 25JRRA442 and 25JRRA1089) and the Gansu Longyuan Youth Innovation and Entrepreneurship (No. 2025QNTD34).

References

1 F. Song, Y. Zeng, R. Sheng, Y. Lin, X. Wang, C. Hong, G. Luo, Y. Wang, M. Fang, S. He, S. Zhang, Q. Zheng, T. Li, S. Ge, J. Zhang and N. Xia, *ACS Nano*, 2024, **18**, 31809–31822.
2 M. Yang, G. Rao, L. Li, L. Qi, C. Ma, H. Zhang, J. Gong, B. Wei, X. E. Zhang, G. Chen, S. Cao and F. Li, *ACS Nano*, 2024, **18**, 13755–13767.
3 B. S. Ou, O. M. Saouaf, J. Yan, T. U. J. Bruun, J. Baillet, X. Zhou, N. P. King and E. A. Appel, *Adv. Healthcare Mater.*, 2023, **12**, e2301495.
4 J. H. Lee, H. J. Sutton, C. A. Cottrell, I. Phung, G. Ozorowski, L. M. Sewall, R. Nedellec, C. Nakao, M. Silva, S. T. Richey, J. L. Torres, W. H. Lee, E. Georgeson, M. Kubitz, S. Hodges, T. M. Mullen, Y. Adachi, K. M. Cirelli, A. Kaur, C. Allers, M. Fahlberg, B. F. Grasperge, J. P. Dufour, F. Schiro, P. P. Aye, O. Kalyuzhniy, A. Liguori, D. G. Carnathan, G. Silvestri, X. Shen, D. C. Montefiori, R. S. Veazey, A. B. Ward, L. Hangartner, D. R. Burton, D. J. Irvine, W. R. Schief and S. Crotty, *Nature*, 2022, **609**, 998–1004.
5 X. Dong, P. Pan, Q. Zhang, J. J. Ye and X. Z. Zhang, *Nano Lett.*, 2023, **23**, 1219–1228.
6 Q. Yin, W. Luo, V. Mallajosyula, Y. Bo, J. Guo, J. Xie, M. Sun, R. Verma, C. Li, C. M. Constantz, L. E. Wagar, J. Li, E. Sola, N. Gupta, C. Wang, O. Kask, X. Chen, X. Yuan, N. C. Wu, J. Rao, Y. H. Chien, J. Cheng, B. Pulendran and M. M. Davis, *Nat. Mater.*, 2023, **22**, 380–390.
7 J. Deng, Z. Wang, L. Wu, Z. Song, H. S. Bahlol, X. Li, L. Zhao and H. Han, *ACS Nano*, 2025, **19**, 9042–9052.
8 W. Fu, Z. F. Sabet, J. Liu, M. You, H. Zhou, Y. Wang, Y. Gao, J. Li, X. Ma and C. Chen, *Nanoscale*, 2020, **12**, 7960–7968.
9 X. Li, Y. Wang, S. Wang, C. Liang, J. Pu, Y. Chen, L. Wang, H. Xu, Y. Shi and Z. Yang, *Nanoscale*, 2020, **12**, 2111–2117.
10 E. C. Gale, A. E. Powell, G. A. Roth, E. L. Meany, J. Yan, B. S. Ou, A. K. Grosskopf, J. Adamska, V. Picece, A. I. d'Aquino, B. Pulendran, P. S. Kim and E. A. Appel, *Adv. Mater.*, 2021, **33**, e2104362.
11 H. Hao, S. Wu, J. Lin, Z. Zheng, Y. Zhou, Y. Zhang, Q. Guo, F. Tian, M. Zhao, Y. Chen, X. Xu, L. Hou, X. Wang and R. Tang, *Nat. Biomed. Eng.*, 2023, **7**, 928–942.
12 J. R. Adams, S. L. Haughney and S. K. Mallapragada, *Acta Biomater.*, 2015, **14**, 104–114.
13 H. Jia, J. Lin, D. Wang, X. Lv, Q. Wang, Z. Wang, J. Liu, L. Yang and J. Liu, *Adv. Funct. Mater.*, 2024, **34**, 2315442.
14 R. Zhong, S. Talebian, B. B. Mendes, G. Wallace, R. Langer, J. Conde and J. Shi, *Nat. Mater.*, 2023, **22**, 818–831.
15 T. Guan, Z. Chen, X. Wang, S. Gao, X. Lu, Y. Li, Z. Wang, S. Zhang, Y. Guo, M. Guo, Y. Cui, Y. Wang and C. Chen, *J. Am. Chem. Soc.*, 2025, **147**, 6523–6535.

16 M. Kabiri, I. Bushnak, M. T. McDermot and L. D. Unsworth, *Biomacromolecules*, 2013, **14**, 3943–3950.
17 M. Rosa, E. Gallo, P. Pellegrino, F. A. Mercurio, M. Leone, M. Cascione, B. Carrese, G. Morelli, A. Accardo and C. Diaferia, *ACS Appl. Bio Mater.*, 2025, **8**, 488–502.
18 Y. Si, Q. Tian, F. Zhao, S. H. Kelly, L. S. Shores, D. F. Camacho, A. I. Sperling, M. S. Andrade, J. H. Collier and A. S. Chong, *Sci. Adv.*, 2020, **6**, eaba0995.
19 J. S. Rudra, Y. F. Tian, J. P. Jung and J. H. Collier, *Proc. Natl. Acad. Sci. U. S. A.*, 2010, **107**, 622–627.
20 J. S. Rudra, T. Sun, K. C. Bird, M. D. Daniels, J. Z. Gasiorowski, A. S. Chong and J. H. Collier, *ACS Nano*, 2012, **6**, 1557–1564.
21 H. Wang, Z. Luo, Y. Wang, T. He, C. Yang, C. Ren, L. Ma, C. Gong, X. Li and Z. Yang, *Adv. Funct. Mater.*, 2016, **26**, 1822–1829.
22 Z. Luo, Q. Wu, C. Yang, H. Wang, T. He, Y. Wang, Z. Wang, H. Chen, X. Li, C. Gong and Z. Yang, *Adv. Mater.*, 2017, **29**, 1601776.
23 C. Liang, X. Yan, R. Zhang, T. Xu, D. Zheng, Z. Tan, Y. Chen, Z. Gao, L. Wang, X. Li and Z. Yang, *J. Controlled Release*, 2020, **317**, 109–117.
24 K. Chen, X. Wu, Q. Wang, Y. Wang, H. Zhang, S. Zhao, C. Li, Z. Hu, Z. Yang and L. Li, *Chin. Chem. Lett.*, 2023, **34**, 107446.
25 T. Guan, J. Li, C. Chen and Y. Liu, *Adv. Sci.*, 2022, **9**, 1–26.
26 Y. Zhao, Z. Li, J. Voyer, Y. Li and X. Chen, *ACS Appl. Mater. Interfaces*, 2022, **14**, 21872–21885.
27 H. Guo, S. Sun, Y. Jin, S. Yang, Y. Wei, D. Sun, S. Yin, J. Ma, Z. Liu, J. Guo, J. Luo, H. Yin, X. Liu and D. Liu, *Vet. Res.*, 2013, **44**, 1–13.
28 F. Eweje, V. Ibrahim, A. Shajii, M. L. Walsh, K. Ahmad, A. Alrefai, D. Miyasato, J. R. Davis, H. Ham, K. Li, M. Roehrl, C. A. Haller, D. R. Liu, J. Chen and E. L. Chaikof, *Nat. Biotechnol.*, 2025, DOI: 10.1038/s41587-025-02664-2.
29 C. Korupalli, W. Y. Pan, C. Y. Yeh, P. M. Chen, F. L. Mi, H. W. Tsai, Y. Chang, H. J. Wei and H. W. Sung, *Biomaterials*, 2019, **216**, 119268.
30 J. Zhou, Z. Wang, C. Yang, H. Zhang, M. S. Fareed, Y. He, J. Su, P. Wang, Z. Shen, W. Yan and K. Wang, *Acta Biomater.*, 2022, **151**, 223–234.
31 J. Zhou, R. Cha, Z. Wu, C. Zhang, Y. He, H. Zhang, K. Liu, M. S. Fareed, Z. Wang, C. Yang, Y. Zhang, W. Yan and K. Wang, *Nano Today*, 2023, **49**, 101801.
32 J. Zhou, H. Zhang, M. S. Fareed, Y. He, Y. Lu, C. Yang, Z. Wang, J. Su, P. Wang, W. Yan and K. Wang, *ACS Nano*, 2022, **16**, 7636–7650.
33 F. Cao, G. Ma, M. Song, G. Zhu, L. Mei and Q. Qin, *Soft Matter*, 2021, **17**, 4445–4451.
34 Y. Tian, H. Wang, Y. Liu, L. Mao, W. Chen, Z. Zhu, W. Liu, W. Zheng, Y. Zhao, D. Kong, Z. Yang, W. Zhang, Y. Shao and X. Jiang, *Nano Lett.*, 2014, **14**, 1439–1445.
35 R. Mourtada, H. D. Herce, D. J. Yin, J. A. Moroco, T. E. Wales, J. R. Engen and L. D. Walensky, *Nat. Biotechnol.*, 2019, **37**, 1186–1197.
36 M. Wang, J. Wang, P. Zhou, J. Deng, Y. Zhao, Y. Sun, W. Yang, D. Wang, Z. Li, X. Hu, S. M. King, S. E. Rogers, H. Cox, T. A. Waigh, J. Yang, J. R. Lu and H. Xu, *Nat. Commun.*, 2018, **9**, 5118.
37 S. Chen, Z. Li, C. Zhang, X. Wu, W. Wang, Q. Huang, W. Chen, J. Shi and D. Yuan, *Small*, 2023, **19**, e2301063.
38 L. Wang, L. Duan, G. Liu, J. Sun, M. A. Shahbazi, S. C. Kundu, R. L. Reis, B. Xiao and X. Yang, *Adv. Sci.*, 2023, **10**, e2207352.
39 V. H. Giang Phan, H. T. T. Duong, T. Thambi, T. L. Nguyen, M. H. Turabee, Y. Yin, S. H. Kim, J. Kim, J. H. Jeong and D. S. Lee, *Biomaterials*, 2019, **195**, 100–110.
40 K. S. Cruz-Amaya, D. Hernández-Martínez, C. L. Del-Toro-Sánchez, E. Carvajal-Millan, K. Martínez-Robinson, Y. B. DeAnda-Flores and Y. I. Cornejo-Ramírez, *ACS Omega*, 2024, **9**, 28564–28576.
41 W. Ji, C. Yuan, P. Chakraborty, P. Makam, S. Bera, S. Rencus-Lazar, J. Li, X. Yan and E. Gazit, *ACS Nano*, 2020, **14**, 7181–7190.
42 J. Wojciechowski, A. D. Martin, E. Y. Du, C. J. Garvey, R. E. Nordon and P. Thordarson, *Nanoscale*, 2020, **12**, 8262–8267.
43 Y. Du, T. Song, J. Wu, X. D. Gao, G. Ma, Y. Liu and Y. Xia, *Biomaterials*, 2022, **280**, 121313.
44 W. Tao, X. Wu, J. Li, F. Wu, C. Chen, T. Jiang, C. Xu, S. Jiang, J. Wang, B. Xiao, Y. Du and S. Zhang, *Chem. Eng. J.*, 2024, **479**, 147437.
45 J. Mondal, K. Chakraborty, E. J. Bunggulawa, J. M. An, V. Revuri, M. Nurunnabi and Y. K. Lee, *J. Controlled Release*, 2024, **372**, 1–30.
46 W. Fu, M. Guo, X. Zhou, Z. Wang, J. Sun, Y. An, T. Guan, M. Hu, J. Li, Z. Chen, J. Ye, X. Gao, G. F. Gao, L. Dai, Y. Wang and C. Chen, *ACS Nano*, 2024, **18**, 11200–11216.
47 D. Qiao, L. Li, L. Liu and Y. Chen, *ACS Appl. Mater. Interfaces*, 2022, **14**, 50592–50600.
48 W. Yin, Z. Xu, C. Chang, Y. Zhao, H. Wang, J. Zhang, F. Ma, X. Zuo, B. Tang and Y. Lu, *Mater. Horiz.*, 2024, **11**, 2153–2168.
49 W. Luo, Z. Yang, J. Zheng, Z. Cai, X. Li, J. Liu, X. Guo, M. Luo, X. Fan, M. Cheng, T. Tang, J. Liu and Y. Wang, *ACS Nano*, 2024, **18**, 28894–28909.
50 H. Song, Q. Su, Y. Nie, C. Zhang, P. Huang, S. Shi, Q. Liu and W. Wang, *Acta Biomater.*, 2023, **158**, 535–546.
51 Z. Liu, J. He, T. Zhu, C. Hu, R. Bo, A. Wusiman, Y. Hu and D. Wang, *ACS Appl. Mater. Interfaces*, 2020, **12**, 39014–39023.
52 H. Jia, Y. Shang, H. Cao, Y. Gao, J. Liu, L. Yang, C. Yang, C. Ren, Z. Wang and J. Liu, *Chem. Eng. J.*, 2022, **435**, 134782.
53 Y. Zhao, X. Zhao, X. Wang, Z. Ma, J. Yan, S. Li, N. Wang, J. Jiao, J. Cui and G. Zhang, *Acta Biomater.*, 2025, **193**, 417–428.
54 P. Wang, Y. Wang, H. Li, M. Wang, Y. Wang, X. Wang, L. Ran, H. Xin, J. Ma, G. Tian, W. Gao and G. Zhang, *Acta Biomater.*, 2024, **177**, 400–413.

55 Z. Xiao, D. Wang, C. Wang, Z. Chen, C. Huang, Y. Yang, L. Xie, L. Zhang, L. Xu, M. R. Zhang, K. Hu, Z. Li and L. Luo, *Mater. Today Bio*, 2022, **15**, 100297.
56 S. Meulewaeter, I. Aernout, J. Deprez, Y. Engelen, M. De Velder, L. Franceschini, K. Breckpot, S. Van Calenbergh, C. Asselman, K. Boucher, F. Impens, S. C. De Smedt, R. Verbeke and I. Lentacker, *J. Controlled Release*, 2024, **370**, 379–391.
57 B. Wu, J. Liang, X. Yang, Y. Fang, N. Kong, D. Chen and H. Wang, *J. Am. Chem. Soc.*, 2024, **146**, 8585–8597.
58 M. Zhao, C. He, X. Zheng, M. Jiang, Z. Xie, H. Wei, S. Zhang, Y. Lin, J. Zhang and X. Sun, *J. Controlled Release*, 2024, **369**, 556–572.
59 Y. Sun, Y. Gao, T. Su, L. Zhang, H. Zhou, J. Zhang, H. Sun, J. Bai and P. Jiang, *ACS Nano*, 2025, **19**, 852–870.